

# Characterizing the Orbital Eccentricities of Transiting Extrasolar Planets with Photometric Observations

Eric B. Ford<sup>1,2,3</sup>, Samuel N. Quinn<sup>2</sup>, Dimitri Veras<sup>3,4,5</sup>

## ABSTRACT

The discovery of over 200 extrasolar planets with the radial velocity (RV) technique has revealed that many giant planets have large eccentricities, in striking contrast with most of the planets in the solar system and prior theories of planet formation. The realization that many giant planets have large eccentricities raises a fundamental question: “Do terrestrial-size planets of other stars typically have significantly eccentric orbits or nearly circular orbits like the Earth?” Here, we demonstrate that photometric observations of transiting planets could be used to characterize the orbital eccentricities for individual transiting planets, as well the eccentricity distribution for various populations of transiting planets (e.g., those with a certain range of orbital periods or physical sizes). Such characterizations can provide valuable constraints on theories for the excitation of eccentricities and tidal dissipation. We outline the future prospects of the technique given the exciting prospects for future transit searches, such as those to be carried out by the CoRoT and Kepler missions.

*Subject headings:* planetary systems — planetary systems: formation — planets and satellites: general — techniques: photometric — methods: statistical — celestial mechanics

---

<sup>1</sup>Hubble Fellow

<sup>2</sup>Harvard-Smithsonian Center for Astrophysics, Mail Stop 51, 60 Garden Street, Cambridge, MA 02138, USA

<sup>3</sup>Department of Astronomy, University of Florida, 211 Bryant Space Science Center, P.O. Box 112055, Gainesville, FL 32611-2055, USA

<sup>4</sup>JILA, Campus Box 440, University of Colorado, Boulder, CO 80309, USA

<sup>5</sup>Department of Astrophysical and Planetary Sciences, University of Colorado, Boulder, CO 80309, USA

## 1. Introduction

Theorists have proposed numerous mechanisms that could excite orbital eccentricities. Some of these mechanisms are expected to affect all planets independent of their mass (e.g., perturbations by binary companions, passing stars, or stellar jets; e.g., Holman et al. 1997; Laughlin & Adams 1998; Ford et al. 2000; Zakamska & Tremaine 2004; Namouni 2007), while the efficiency of other mechanisms would vary with planet mass (e.g., planet-disk or planet-planet interactions; e.g., Artymowicz 1992; Goldreich & Sari 2003; Chatterjee et al. 2007). If the mechanism(s) exciting eccentricities of the known giant planets also affect terrestrial planets, then Earth-mass planets on nearly circular orbits could be quite rare. On the other hand, if large eccentricities are common only in systems with massive giant planets and/or very massive disks, then there may be an abundance of planetary systems with terrestrial planets on low eccentricity orbits (Beer et al. 2004). Thus, understanding the eccentricity distribution of terrestrial planets could provide empirical constraints for planet formation theories (e.g., Ford & Rasio 2007) and shed light on the processes that determined the eccentricity evolution in our solar system. Since the discovery of transiting giant planets with eccentric orbits, authors have begun to consider the implications of eccentricities for transiting planets (e.g., Barnes 2007; Burke 2008).

The CoRoT and Kepler space missions are expected to detect many transiting planets and measure their sizes and orbital periods, including some in or near the “habitable zone” (e.g., Kasting et al. 1993). The Kepler mission aims to determine the frequency of Earth-like planets, and study how the frequency and properties of planets correlates with the properties of their host stars (Basri et al. 2005). Since a significant eccentricity would cause the stellar flux incident on the planet’s surface to vary, a planet’s eccentricity affects its climate (i.e., equilibrium temperature, amplitude of seasonal variability) and potentially its habitability (Williams et al. 2002; Gaidos & Williams 2004). Our method could be applied to these planets to determine the frequency of terrestrial planets that could also have Earth-like climates, and thus influence the design of future space missions that will attempt to detect and characterize nearly Earth-like planets (e.g., Space Interferometry Mission-PlanetQuest) and search them for signs of life (e.g., Terrestrial Planet Finder).

In §2, we show how the duration of a transit is affected by a planet’s orbital eccentricity. We outline how to interpret the transit duration for transiting planets with both low signal-to-noise light curves (§2.1.1) and high signal-to-noise (§2.1.2). We compare the magnitude of the effect on the transit duration to the expected precision of eccentricity constraints based on Kepler photometric data (§2.2) and also the typical accuracy of stellar parameters (§2.3). We demonstrate that Kepler observations could be used to characterize the orbital eccentricities of terrestrial planets. We describe statistical approaches for analyzing the distribution of

transit durations of a population of transiting planets in §3. In §3.4, we discuss the role of radial velocity observations for constraining eccentricities of Earth-like transiting planets. In §4, we conclude with a discussion of how the results could contribute to understanding the formation and evolution of terrestrial planets and address fundamental questions, such as “What is the frequency of terrestrial planets that have Earth-like eccentricities?” and “What is the frequency of terrestrial planets that pass through the habitable zone?”

## 2. Light Curve of an Eccentric Transiting Planet

The total transit duration is defined as the time interval between the first and fourth points of contact (Fig. 1). In the approximation that the mean planet-star separation ( $a$ ) is much greater than both the stellar radius ( $R_\star$ ) and the planetary radius ( $R_p$ ), the transit duration is much less than the orbital period ( $P$ ), and thus the planet-star separation during the transit ( $d_t$ ) is nearly constant. Using these approximations, the total transit duration ( $t_D$ ) is given by

$$\frac{t_D}{P} \simeq \frac{R_\star}{\pi a \sqrt{1-e^2}} \sqrt{(1+r)^2 - b^2} \left( \frac{d_t}{a} \right), \quad (1)$$

where  $e$  is the orbital eccentricity,  $r \equiv R_p/R_\star$  is the ratio of the planet radius to stellar radius,  $b \equiv d_t \cos i/R_\star$  is the impact parameter, and  $i$  is the orbital inclination measured relative to the plane of the sky (Tingley & Sackett 2005). The planet-star separation at the time of transit is given by  $d_t = a(1 - e \cos E_t) = a(1 - e^2)/(1 + e \cos T_t) = a(1 - e^2)/(1 + e \cos \omega)$ , where  $T_t$  and  $E_t$  are the true and eccentric anomalies at the time of transit, and  $\omega$  is the argument of periastron measured relative to the line of sight. (Note that this differs from the convention for radial velocity determinations.) Thus, the ratio of the actual transit duration to the transit duration for the same planet on a circular orbit (assuming other transit parameters such as size and impact parameter are held fixed) is  $(1 + e \cos \omega)/\sqrt{1 - e^2}$ . We have performed numerical integrations to verify that this approximation is accurate to better than  $\simeq 0.1\%$ , for eccentricities as high as 0.95 (Fig. 2).

We define the variable  $\tau_b \equiv d_t/(a\sqrt{1-e^2})$  to be the ratio of the transit duration of one planet to the transit duration for an identical planet with the same orbital period and impact parameter, but on a circular orbit. In general, transiting planets could have significant eccentricities, in which case  $\tau_b$  will deviate from unity (e.g.,  $\tau_b \simeq 1.8$  for HAT-P2b; Bakos et al. 2007). For planets on low eccentricity orbits,  $|\tau_b - 1| \simeq O(e)$ . For large eccentricities,  $\tau_b$  can range from zero to several (Fig. 2). For the case of a central transit of an Earth-like

planet orbiting a solar-mass star on a circular orbit,

$$t_D \simeq 13\text{hours} \left(\frac{P}{\text{yr}}\right)^{1/3} \left(\frac{R_\star}{R_\odot}\right) \left(\frac{M_\odot}{M_\star}\right)^{1/3} (1 + \mu)^{-1/3} ((1 + r)^2 - b^2)^{1/2} \tau_b, \quad (2)$$

where  $M_\star$  is the stellar mass and  $\mu \equiv m_p/M_\star$  is the planet-star mass ratio. The planet-star mass ratio ( $\mu \equiv m_p/M_\star$ ) is typically negligible for planetary companions. (If it is large, then it could be measured by obtaining RV observations.) By assuming that the pericenter direction is randomly oriented relative to the line of sight, we can compute the probability distribution for  $\tau_b$  as a function of eccentricity (Fig. 3).

## 2.1. Analysis of Transiting Planet Light Curves

Here we outline the basics of how photometric light curves can be used to constrain the eccentricities of transiting planets. We discuss two limiting regimes: 1) low signal-to-noise (S/N) light curves that provide no constraint on the impact parameter, and 2) high S/N light curves that measure the impact parameter.

### 2.1.1. Impact Parameter Not Measured (Low S/N)

For any transit detection, photometric observations alone directly measure the orbital period ( $P$ ), the total transit duration ( $t_D$ ), and the depth of the transit. For the purposes of providing analytic estimates, we neglect the effects of limb darkening, so that the transit depth is given by the planet-star area ratio ( $r^2$ ). For some faint stars and/or small planets, it may be difficult to measure additional light curve parameters such as the ingress duration and the impact parameter. For these cases, the total transit duration,  $t_D$ , can be compared to  $t_{D,o}$ , the transit duration expected for the same planet with the same orbital period ( $P$ ) and mean stellar density ( $\rho_\star$ ), but assuming a circular orbit and central transit ( $b = 0$ ). Even for transiting planets with low S/N light curves, photometric observations can measure the ratio

$$\tau_o \equiv \frac{t_D}{t_{D,o}} = \left(\frac{d_t}{a\sqrt{1-e^2}}\right) \left(\frac{\sqrt{(1+r)^2 - b^2}}{1+r}\right) \simeq \left(\frac{t_D}{13\text{hours}}\right) \left(\frac{\text{yr}}{P}\right)^{1/3} \left(\frac{\rho_\star}{\rho_\odot}\right)^{1/3} \frac{(1+\mu)^{1/3}}{(1+r)}. \quad (3)$$

Since  $\mu = m_p/M_\star \ll 1$  for planetary mass companions, a value of  $\tau_o$  significantly greater than unity can only arise for an eccentric planet, but a value of  $\tau_o$  less than unity could be due to either a non-central transit ( $b > 0$ ) or a non-zero eccentricity ( $e > 0$ ). Thus, it is not

possible to measure the eccentricity for an individual planet with only low S/N photometry. However, it is still possible to characterize the distribution of eccentricities for a population of planets based on the observed distribution of  $\tau_o$  (see §3.2). Since the above analysis can be applied to relatively faint stars with low S/N transit light curves, we expect that Kepler will discover many planets that can be included in statistical analyses of  $\tau_o$  (Basri et al. 2005). We note the actual analysis should consider the effects of limb darkening, which cause the depth of a high-latitude transit relative to be greater than a than an equatorial transit even for the same star-planet area ratio. While limb darkening precludes simple analytic expressions, such effects can be incorporated into Monte Carlo simulations.

In §3, we will show that Kepler observations could constrain the *distribution of eccentricities* and reject plausible eccentricity distributions for terrestrial planets. The precision of the eccentricity constraints will depend on the precision and accuracy of the measurements of  $\tau_o$ . In §2.2 we show that the the orbital period, transit depth, and transit duration can be measured with sufficient precision that the accuracy for the measured  $\hat{\tau}_o$  will typically be limited by the deviation of the inferred stellar density ( $\hat{\rho}_*$ ) from the actual stellar density ( $\rho_*$ ), i.e.,  $\hat{\tau}_o \simeq \tau_o(\hat{\rho}_*/\rho_*)^{1/3}$ . The mean stellar density could be estimated using spectroscopy and stellar modeling (§2.3), resulting in a typical accuracy for  $\hat{\tau}_o$  of  $\sim 5 - 15\%$  (e.g., Ford et al. 1999; Fischer & Valenti 2005; Takeda et al. 2007). The spread of transit durations due to the unknown inclination will have a negligible effect on the ability of low S/N transit light curves to constrain the eccentricity distribution.

### 2.1.2. Impact Parameter Measured (High S/N)

For high-quality light curves, photometric observations can measure the time of each point of contact and determine both the total transit duration ( $t_D$ ) and  $t_F$  (Fig. 1). If we neglect limb darkening, then the impact parameter can be determined by the photometric observables,  $b^2 = [(1 - r)^2 - \gamma^2(1 + r)^2] / (1 - \gamma^2)$ , where we define  $\gamma^2 \equiv t_F^2/t_D^2$  (Seager & Mallen-Ornelas 2003).

In practice, the transit shape will be affected by limb darkening (Fig. 4) and we must fit for the limb darkening parameters to determine the impact parameter (and planet-star radius ratio). Previous experience analyzing transit photometry of giant planets has found that the limb darkening parameters can be accurately estimated with stellar models and the uncertainty in limb darkening parameters typically introduces relatively modest additional uncertainties and have only small correlations with the other model parameters of interest (e.g., Brown et al. 2001; Holman et al. 2006; Burke et al. 2007; Knutson et al. 2007; Winn et al. 2007; Torres et al. 2008). In order to verify that the uncertainty in limb darkening

coefficients will introduce only modest additional uncertainties, we have generated simulated Kepler V-band light curves for terrestrial planets transiting a  $V = 12$  magnitude solar-like star, including a quadratic limb darkening model (Mandell & Agol 2002; Claret 2000). We then calculate  $\Delta\chi^2$ , varying the transit time, transit duration, the planet size, impact parameter, and quadratic limb darkening coefficients (see Fig. 5). While these are some modest correlations between the transit duration and limb darkening parameters, these correlations are a much smaller effect than the uncertainty due to the correlation between the transit duration and the impact parameter. Therefore, we conclude that the uncertainty in impact parameter will be the limiting factor and we can neglect the effects of limb darkening when estimating the power of transit durations for constraining the eccentricities of transiting planets (see §3.2). Once the host star and transit time are known from Kepler observations, a future transit can be observed using ground-based observatories at multiple wavelengths. By combining the inferred stellar properties with limb darkening profiles from stellar models, one can determine the impact parameter from even relatively low precision data (e.g., Jha et al. 2000). Infrared observations would be particularly useful, as they minimize the effects of limb darkening and aid in the measurement of the impact parameter. Since the impact parameter is the same at all wavelengths, ground-based transit light curves could effectively eliminate the need to fit for this parameter when analyzing the Kepler photometry. Here, we assume that limb-darkening parameters can be well constrained by some combination of stellar modeling and external observations.

For systems with high S/N photometry, the total transit duration,  $t_D$ , can be compared to  $t_{D,b}$ , the transit duration expected for the same planet and star with the same observed orbital period, impact parameter ( $b$ ), and mean stellar density, but assuming a circular orbit. Then, Kepler can measure the ratio

$$\tau_b = \frac{t_D}{t_{D,b}} \simeq \left( \frac{t_D}{13\text{hours}} \right) \left( \frac{yR}{P} \right)^{1/3} \left( \frac{1 - \gamma^2}{r} \right)^{1/2} \left( \frac{\rho_\star}{\rho_\odot} \right)^{1/3} (1 + \mu)^{1/3}. \quad (4)$$

The fact that the planet is transiting the star places a constraint on a combination of true anomaly and the direction of pericenter. Therefore, the actual value of  $\tau_b$  depends only on the eccentricity and direction of pericenter, and  $\tau_b$  can be measured using a combination of transit photometry and stellar parameters (e.g., from spectroscopy and stellar modeling). Using high S/N photometry, we can accurately measure the first three terms on the right hand side of Eqn. 4. The last term containing the planet-star mass ratio ( $\mu$ ) is negligible for planetary companions. Therefore, the accuracy of the measured  $\tau_b$  will typically be limited by the uncertainty in the cube root of the mean stellar density ( $\sigma_{\rho_\star^{1/3}}$ ). We can detect a non-zero eccentricity for an individual planet when  $e > \sigma_{\rho_\star^{1/3}} / \rho_\star^{1/3} \simeq 0.05 - 0.15$  (§2.3). This is quite significant given the mean eccentricity of planets discovered by RV surveys is  $\simeq 0.3$

(ignoring planets with  $P < 10$  days that may have been influenced by tidal circularization; Butler et al. 2006).

## 2.2. Expected Precision of Kepler Measurements

Here we present estimates of the timing precision possible with Kepler observations, assuming a flux measurement precision of  $\sigma_{ph} \simeq 400$ ppm during a one minute integration on a  $V=12$  star and uncertainties that scale with the square root of the photon count (Basri et al. 2005). For the sake of deriving approximate analytic expressions, we assume uncorrelated Gaussian uncertainties and ignore complications due to limb darkening in this paper

To determine the precision of eccentricity constraints, we must estimate the precision of the constraints from transit photometry. The fractional transit depth ( $r^2$  in the absence of limb darkening) can be measured with a precision,  $\sigma_{r^2} \simeq \sigma_{ph}/\sqrt{t_F \Lambda N_{tr}}$ , where  $\Lambda$  is the rate of photometric measurements with precision  $\sigma_{ph}$  and  $N_{tr} \simeq 4(\text{yr}/P)$  is the number of transits observed during the four year mission lifetime. Note that in this approximation the precision does not depend on the integration time, provided that it is significantly less than the ingress/egress time. In practice, an increased rate of measurements is valuable for constraining any brightness variations across the stellar disk (e.g., limb darkening, star spots, plage).

The time of each ingress/egress ( $t_{in/out}$ ) can be measured with a precision  $\sigma_{t_{in/out}} \simeq \sigma_{ph} \sqrt{\Delta t_{in/out}/\Lambda} (R_*/R_p)^2$ , where  $\Delta t_{in/out}$  is the duration of ingress/egress (Ford & Gaudi 2006). Therefore, the sidereal orbital period can be measured with a precision of  $\sigma_P \simeq \sigma_{t_{in/out}}/\sqrt{2(N_{tr}-1)}$  and the duration of the transit can be measured with a precision of  $\sigma_{t_D} = \sigma_{t_{in/out}} \sqrt{2/N_{tr}}$ . Once there are at least two transits, the uncertainty in  $t_D$  will dominate.

The duration of ingress ( $\Delta t_{in}$ ) or egress ( $\Delta t_{out}$ ) is given by  $\Delta t_{in/out} \equiv \epsilon t_D$ , where  $\epsilon(1-\epsilon) = r/[(1+r)^2 - b^2]$ . For non-grazing transits,  $\epsilon \ll 1$ , so the ingress/egress duration is

$$\Delta t_{in} \simeq \Delta t_{out} \simeq 7.1 \text{minutes} \left(\frac{R_p}{R_\oplus}\right) \left(\frac{P}{\text{yr}}\right)^{\frac{1}{3}} ((1+r)^2 - b^2)^{\frac{-1}{2}} \left(\frac{M_\odot}{M_\star}\right)^{\frac{1}{3}} (1+\mu)^{\frac{-1}{3}} \tau_b. \quad (5)$$

Inserting fiducial values for a target star with an apparent magnitude of  $V$ , we expect a fractional precision for the mean transit duration of an individual planet to be

$$\frac{\sigma_{t_D}}{t_D} \simeq 0.013 \left(\frac{P}{\text{yr}}\right)^{\frac{1}{3}} \left(\frac{R_p}{R_\oplus}\right)^{\frac{-3}{2}} \left(\frac{R_\star}{R_\odot}\right) \left(\frac{M_\star}{M_\odot}\right)^{\frac{1}{6}} (1+\mu)^{\frac{1}{6}} \tau_b^{\frac{-1}{2}} ((1+r)^2 - b^2)^{\frac{-3}{4}} 10^{(V-12)/5}. \quad (6)$$

For a Jupiter-sized planet with a similar orbit and host star, the expected fiducial fractional uncertainty for Kepler observations decreases to  $\simeq 3 \times 10^{-4}$ . Ground-based observatories have achieved a precision of  $\sigma_{t_D}/t_D \simeq 1.5\%$  for short-period giant planets (e.g., Holman et al. 2007).

For modest eccentricities, Kepler’s expected measurement precision will place a lower limit on the uncertainty of a given planet’s eccentricity ( $\sigma_e$ ) of order  $\simeq \sigma_{t_D}/t_D$ . Even for Earth-sized planets around V=14 stars, Kepler is expected to achieve the photometric precision necessary to measure eccentricities as low as  $\simeq 0.03$ .

For the sake of completeness, we also estimate one additional timescale. For an eccentric orbit, there is a slight change in  $d_t$  between ingress and egress that results in a difference between the ingress and egress durations,

$$\Delta t_{in} - \Delta t_{out} \simeq 4\text{sec} \left(\frac{P}{\text{yr}}\right)^{-1/3} \left(\frac{R_p}{R_\oplus}\right) \left(\frac{R_\star}{R_\odot}\right) \left(\frac{M_\odot}{M_\star}\right)^{2/3} \left(\frac{(1+\mu)^{-2/3} e \sin T_t}{(1-b^2)(1+e \cos T_t)(1-e^2)^{3/2}}\right), \quad (7)$$

where  $T_t$  is the true anomaly at the time of mid-transit and we have neglected the second order effect of change in the impact parameter. For a Jupiter-sized planet with a 4 day orbit around a solar-sized star, the difference in ingress and egress durations increases to 3.4 minutes. While Kepler and/or high-precision follow-up observations might be able to measure such effects for a relatively small number of bright stars, we expect other methods will typically provide more powerful constraints on the eccentricity.

### 2.3. Uncertainties in Stellar Mass and Radius

For many transiting planets photometric observations will be so precise that uncertainties in the stellar properties will limit the accuracy of  $\hat{\tau}_o$  or  $\hat{\tau}_b$  and hence the eccentricity constraints (unless there are significant constraints from RV observations or time of secondary transit; see §3.4). From the perspective of stellar modeling, the physical properties of a star (e.g., radius, and density) are a function of at least three key variables: stellar mass, composition, and age. Hence stellar modeling can only provide powerful constraints on the star’s physical properties if there are at least three observational constraints. The effective temperature ( $T_{\text{eff}}$ ) and metallicity ( $[Fe/H]$ ) can be accurately derived from a single high-precision spectroscopic observation. When a precise parallax ( $\pi$ ) is available, the stellar luminosity ( $L_\star$ ) can be calculated from the apparent magnitude (V; and a bolometric correction). The three constraints ( $T_{\text{eff}}$ ,  $[Fe/H]$ ,  $L_\star$ ) can be combined with stellar evolution tracks to determine the stellar mass, radius, density, etc. (e.g., Ford et al. 1999), with some well-known degeneracies (e.g., hook region). For relatively bright and nearby stars



in the California and Carnegie Planet Search and Hipparcos catalog, this method has been used to estimate stellar parameters such as the mass and radius (Valenti & Fischer 2005; Takeda et al. 2007). We applied the Bayesian stellar parameter estimation code of Takeda et al. (2007) to calculate density directly from the joint posterior distribution, accounting for correlations between parameters and the non-linear transformation between observable and derived quantities. We find that this method can determine the mean stellar density with an accuracy of  $\simeq 4 - 10\%$ , with random uncertainties dominated by the parallax.

We caution that there may also be systematic uncertainties due to the stellar evolutionary tracks. Such systematic effects could lead to  $\tau_o$  or  $\tau_b$  being systematically over- or under-estimated and that the error could be highly correlated with the stellar type or other stellar parameters. Ideally, such systematics would be mitigated if the densities of stellar models were validated by independent observations such as double-lined eclipsing binaries for similar type stars. Both the CoRoT and Kepler missions will contribute to stellar astronomy and are likely to contribute towards improving and testing the precision of stellar models. In the absence of externally validated models, systematic uncertainties in stellar models may limit this technique for systems with small eccentricities. Fortunately, the stellar density enters only to the one third power, so potential systematic effects are unlikely to be significant for most planets that have sizable eccentricities. In practice, the eccentricity analysis should be coupled to a sensitivity analysis that tests whether conclusions are sensitive to the choice of stellar models.

Unfortunately, many target stars for Kepler will be too faint and distant to have well determined parallaxes. One alternative approach is to replace  $L_\star$  with a spectroscopically determined stellar surface gravity ( $\log g$ ). Unfortunately,  $\log g$  is quite difficult to measure precisely. For a high-quality spectroscopic observation (e.g.,  $\sigma_{T_{\text{eff}}} \sim 100\text{K}$  and  $\sigma_{[\text{Fe}/\text{H}]} \sim 0.1\text{dex}$ ), the formal uncertainty in  $\log g$  would typically be  $\sim 0.1\text{dex}$ . Unfortunately, there are typically significant correlations with both  $T_{\text{eff}}$  and  $[\text{Fe}/\text{H}]$  (Valenti & Fischer 2005). For a main sequence solar-type star, the uncertainties in the atmospheric parameters would translate to an uncertainty in  $\rho_\star^{1/3}$  (and hence  $\tau_b$ ) of  $\simeq 8\%$ . In some cases, additional constraints on stellar properties such as rotation rate, strength of Ca HK emission, presence of Li, and/or asteroseismology may be able to further constrain stellar parameters and improve the stellar sensitivity for measuring eccentricities.

### 3. Statistical Methodology

In this section, we outline a few of the statistical approaches that could be applied to translate measurements of  $\tau_o$  and/or  $\tau_b$  into eccentricity constraints. First, we outline

a Bayesian approach to calculating the joint posterior probability distribution for the eccentricity and argument of periastron for individual planets. These constraints would be particularly valuable when combined with additional constraints on dynamical properties of the system. Second, we show that the distribution of normalized transit durations contains significant information about the eccentricity distribution of a population of planets.

### 3.1. Individual Planets

For planets with high signal-to noise transit light curves and well-measured stellar properties, we suggest a Bayesian framework for determining the constraints on the eccentricity and argument of pericenter. To illustrate this method, we adopt non-informative prior probability distributions of  $p(e) = 1$  for  $0 \leq e < 1$ ,  $p(\omega) = 1/(2\pi)$  for  $0 \leq \omega < 1$ , and  $p(\cos i) = 1/2$  for  $-1 \leq \cos i < 1$ . We assume that the observed  $\hat{\tau}_b$  is normally distributed about the true value of  $\tau_b$  (i.e.,  $\hat{\tau}_b \sim N(\tau_b, \sigma_{\tau_b}^2)$ ) with  $\sigma_{\tau_b}$  reflecting the uncertainty in the stellar parameters. In Fig. 6, we show examples of the joint posterior probability distribution for six possible values of  $\hat{\tau}_b$ . Note that in this figure,  $\omega$  is measured relative to the line of sight, not relative to the plane of the sky, as is typical when using radial velocity observations. For actual systems, Markov chain Monte Carlo based simulation methods (Ford 2005, 2006) could be used to calculate posterior probability distributions allowing for parameters with correlated uncertainties and/or non-trivial error distributions (e.g., Holman et al. 2006; Burke et al. 2007; Takeda et al. 2007), as well as eccentric orbits.

### 3.2. Characterizing the Eccentricity Distribution of Transiting Planets

We have performed Monte Carlo simulations to calculate the expected distribution of transit durations for various eccentricity distributions. Here, we consider two limiting cases corresponding to low and high signal-to-noise observations: a) only the transit depth, duration, and orbital period are measured, so that the observed light curve provides no information about the impact parameter (Fig. 7), and b) the time of all four points of contact are measured so that the observed light curve provides a good estimate of the impact parameter (Fig. 8).

### 3.2.1. Impact Parameter Not Measured

While it would be most desirable to measure the eccentricity for each individual planet, this will not always be possible. For some planets (particularly those around faint stars), the light curve will not be measured with sufficient precision to measure the orbital inclination and sufficient high-precision RV observations will be impractical. In these cases, it will still be possible to constrain the mean eccentricity of a population of such planets. Since these challenges will be most common for faint stars, we expect that missions such as CoRoT and Kepler will detect a large number of such planets available for statistical analyses.

We consider the distribution of  $\tau_o \equiv t_D/t_{D,o}$ , where  $t_D$  is the actual transit duration,  $t_{D,o}$  is the transit duration expected for the same planet and star, but assuming a circular orbit ( $e = 0$ ) and central transit ( $b = 0$ ). The distribution for the impact parameter,  $b$ , is determined by assuming that the inclination is distributed isotropically (subject to the constraint that a transit occurs). We also assume that the observed  $\hat{\tau}_o$  is normally distributed about the true value of  $\tau_o$  (i.e.,  $\hat{\tau}_o \sim N(\tau_o, \sigma_{\tau_o}^2)$ ) with  $\sigma_{\tau_o} \simeq 0.05 - 0.15$  due to uncertainty in the stellar parameters (depending on the stellar properties and available follow-up observations). In Fig. 7, we show the distribution of  $\tau_o$  for six eccentricity distributions. In Fig. 9 (right), we plot the mean, standard deviation, and skewness of  $\tau_o$  for an ensemble of planets with a given eccentricity. For planets with a circular orbit and an isotropic distribution of inclinations,  $\tau_o$  will have a mean of  $\simeq 0.79$  and a standard deviation of  $\simeq 0.22$  (Fig. 7, panel a). If we assume a uniform distribution of eccentricities ( $e \sim U[0, 1)$ ), then the mean  $\tau_o$  decreases to 0.64 and the standard deviation increases to 5.2. Alternatively, if we instead assume an eccentricity distribution similar to that observed for giant planets ( $e \sim R(0.3)$ , a Rayleigh distribution with Rayleigh parameter 0.3; Juric & Tremaine 2007), then the mean decreases to  $\simeq 0.74$  and the standard deviation increases to  $\simeq 0.29$ . Therefore, it would be possible to distinguish between all three models with a plausible sample of planets, assuming normally distributed errors and asymptotic scalings for the mean of the distribution, even without measuring any impact parameters or RVs. If we were to use only the mean value of  $\tau_o$ , then we would be ignoring the variances and shape of the distribution. Instead, a Komogorov-Smirnov test can be used to compare the observed distribution of  $\tau_o$  to the  $\tau_o$  distribution predicted by a given model.

To determine how large an observed sample is needed to obtain statistically significant results, we perform Monte Carlo simulations. For each trial, we generate two samples of transiting planets. The first sample represents a hypothetical observed sample of  $N_{pl}$  planets. The second sample is much larger and is used to calculate the predicted distribution of  $\tau_o$  for a given theoretical model. For both samples, we assume an isotropic distribution of viewing angles, i.e.,  $\cos i \sim U[-1, 1)$  and  $\omega \sim U[0, 2\pi)$ . For each trial, we test whether a

Kolmogorov-Smirnov test can reject the null hypothesis that the two distributions of  $\tau_o$  are drawn from a common distribution. For each  $N_{pl}$  we perform several thousand trials; we increase  $N_{pl}$  until we find that the null hypothesis is rejected at the 95% confidence level for at least half of the trials. We present our results in Table 1. Our simulations show that a population of planets on circular orbits ( $e = 0$ ) could be distinguished from either  $e \sim U[0, 1)$  (eccentricities distributed uniformly between zero and unity) or  $e \sim R(0.3)$  (a Rayleigh distribution with Rayleigh parameter of 0.3) by using measurements of  $\tau_o$  for  $N_{pl} \gtrsim 30$  planets, even without measuring any impact parameters or RVs. Distinguishing an observed population with eccentricities distributed as  $e \sim U[0, 1)$  from a model with  $e \sim R(0.3)$ , would require  $N_{pl} \gtrsim 117$  planets. Distinguishing between an observed population with eccentricities distributed as  $e \sim R(0.3)$  rather than a model with  $e \sim U[0, 1)$ , would require  $N_{pl} \gtrsim 174$  planets. The difference is due to the fact that we use a two-sample Kolmogorov-Smirnov test and the sample size for the theoretical model is at least an order of magnitude greater than the sample size for the sample of “observed” planets.

### 3.2.2. Impact Parameter Measured

When high quality photometry measures the impact parameter ( $b$ ), then we can analyze the distribution of  $\tau_b \equiv t_D/t_{D,b}$ , where  $t_{D,b}$  is the transit duration expected for the same planet with the same impact parameter, but assuming a circular orbit. If all transiting planets had a single eccentricity, then the expected mean value of  $\tau_b$  is given by  $\langle \tau_b \rangle \simeq \sqrt{1 - e^2}$  (Tingley & Sackett 2005) and the expected standard deviation is  $\langle \sigma_{\tau_b} \rangle \simeq (1 - e^2)^{3/8} \sqrt{1 - (1 - e^2)^{1/4}}$ . We show the distribution of  $\tau_b$  for several eccentricity distributions in Fig. 8 and plot the mean, standard deviation, and skewness for sample distributions of  $\tau_b$  in Fig. 9 (left). Note that for small eccentricities, the distribution of  $\tau_b$  is strongly peaked, making it possible to perform a significant test of the null hypothesis that terrestrial planets have nearly circular orbits with a small sample size (§3.3). To account for the uncertainty in the stellar parameters, we assume  $\sigma_{\hat{\tau}_b} \simeq 0.05 - 0.15$  and normally distributed errors and asymptotic scalings. Then, it would be possible to distinguish between various models for the eccentricity distribution of observed planets with a few tens of transiting planets (see Table 2). We find that the distribution of  $\tau_b$  provides significant constraints on both the mean and the width of the eccentricity distribution. For example, Monte Carlo simulations using the Kolmogorov-Smirnov test (similar to those described in §3.2.1, but replacing  $\tau_o$  with  $\tau_b$ ) show that distinguishing between two Gaussian eccentricity distributions with mean eccentricities of 0.18 and 0.36 would require  $N_{pl} \gtrsim 30$  planets. Similarly, distinguishing between two Gaussian eccentricity distributions with a common mean of 0.38 and standard deviations of 0.10 and 0.24 would require  $N_{pl} \gtrsim 65$  planets based on a Kolmogorov-Smirnov test and a

95% confidence level. However, it will be very difficult to measure the higher order moments of the eccentricity distribution (see Fig. 10). In Table 2, we list the number of planet required for several additional pairs of eccentricity distributions.

### 3.3. Testing the Null Hypothesis of Circular Orbits for Individual Planets

We are particularly interested in addressing the question, “How frequently are terrestrial planets on nearly circular orbits?” Therefore, we suggest two statistical tests of the null-hypothesis that each planet is on a circular orbit.

#### 3.3.1. *Low S/N Light Curves & Long Duration Transits*

For an eccentric orbit with the transit near apocenter, the transit duration can be significantly greater than would be expected for the observed orbital period. It is possible to measure a minimum eccentricity for long transits, even for low S/N transits and without measuring RV parameters. Since a non-zero impact parameter can only decrease the duration of transit (relative to a central transit), it will be possible to reject the null hypothesis of a circular orbit (and hence detect a non-zero eccentricity) for planets with long duration transits such that  $\tau_o$  or  $\tau_b$  greater than unity. Unfortunately, the geometric probability of a transit occurring is greater for short transits when the planet is closer to the star. Therefore, if eccentric planets are common, then there will be more transits with  $\tau < 1$ . Fortunately, even a small number of long transits can provide significant constraints for the eccentricity distribution.

#### 3.3.2. *High S/N Light Curves & Stellar Models*

For short-period planets that can be assumed to have tidally circularized,  $\tau_b = 1$ , so high precision light curve observations may provide additional constraints on the star’s properties. For example, Holman et al. (2007) measure  $\rho_\star^{1/3}$  to  $\simeq 1.5\%$  accuracy for TrES-2 (V=11.4). When combined with theoretical models, this allows for very accurate determinations of the stellar and planet radii (Sozzetti et al. 2007). This will enable tests of the null-hypothesis that a planet is on a nearly circular orbit. If it is accurate, then the stellar properties would be measured quite precisely and all measurements should be self-consistent. On the other hand, if the planet is actually eccentric, then assuming a circular orbit could result in an inconsistency. For example, by comparing the allowed stellar models to a spectroscopic

measurement of  $\log g$  one could recognize planets with eccentricities exceeding  $\simeq 0.15$  for solar-like stars. Alternatively, the putative location of the star in the  $(T_{\text{eff}}, \rho_*, [\text{Fe}/\text{H}])$  parameter space could be inconsistent with any stellar model (e.g., Sozzetti et al. 2007). The sensitivity of this test will vary significantly with  $T_{\text{eff}}$  and be most powerful for stars slightly cooler than the Sun. Unfortunately, this method is unlikely to be effective for planets with orbital periods larger than a few days, since they may have eccentric orbits.

### 3.4. Role of Radial Velocity Observations

The realization that many giant planets are on eccentric orbits was the result of RV surveys (e.g., Butler et al. 2006 and references therein). Clearly, RV observations can measure orbital eccentricities, provided that there is a sufficient number, phase coverage, and time span of observations with sufficiently high precision (Ford 2005). In fact, the observational constraints from radial velocity observations and the photometric method that we describe are complimentary. Our photometric method is most sensitive for measuring eccentricities of planets if the pericenter direction is pointing towards or away from the observer (Fig. 6). On the other hand, the radial velocity method is most sensitive to measuring eccentricities of planets with pericenter nearly in the plane of the sky (Ford 2005; Laughlin et al. 2005).

Unfortunately, many of the CoRoT and Kepler target stars ( $V \sim 9 - 16$ ) will be much fainter than the typical targets of RV surveys ( $V \sim 5 - 9$ ). Ground-based transit surveys have obtained follow-up RV observations for candidate planets, but typically at a relatively modest precision. While there are plans to obtain RV confirmation of planet candidates identified by CoRoT or Kepler, these observations will require a large investment of telescope time, especially when attempting to detect Earth-mass or even Neptune-mass planets around relatively faint stars. Even when RV observations can confirm terrestrial planet candidates found by CoRoT or Kepler, they will likely make use of the known orbital period and phase to observe at near the extrema of the RV curve. Measuring the eccentricity requires measuring the shape of the curve and hence many observations spread across a broad range of orbital phases. The amplitude of the deviations of the RV curve from that expected for the same planet on a circular orbit is less than the total RV amplitude by a factor of  $e$  (to lowest order in eccentricity). Assuming a single planet with a orbital period known from photometry, a detection of eccentricity for a planet with  $e \simeq 0.3$  will typically require an order of magnitude more observing time than would be required to detect the planet’s total RV amplitude (at the same level of significance and assuming observations nearly evenly distributed in orbital phase). As an additional complication, the RV method measures the reflex velocity of the star induced by all planets, not just one transiting planet. If a star

harbors a (potentially undetected) non-transiting planet with a RV amplitude comparable to or greater than the radial velocity amplitude due to the epicyclic motion of the transiting planet, then RV observations would face an even greater challenge in measuring the transiting planet’s eccentricity. Despite these challenges, we certainly encourage radial velocity observations for constraining eccentricities whenever they are practical.

#### 4. Discussion

We have described how photometric observations can constrain the eccentricities of individual transiting planets and characterize the eccentricity distribution of a population of planets. For each planet, we can test the null hypothesis that it is on a circular orbit and calculate the posterior probability distribution for the eccentricity. A combination of such analyses for several transiting planets could be used to characterize the eccentricity distribution of a population of planets. For example, this method could be used to investigate how the fraction of eccentric orbits varies with the orbital period or physical properties of the star and planet. We expect this type of analysis to become increasingly powerful given the rapidly growing number of known transiting planets.

This type of analysis will be particularly valuable for low-mass transiting planets or transiting planets around faint host stars. In both cases, radial velocity follow-up observations will be extremely challenging. This will be the case for many transiting planet candidates found by space-based transit searches, such as CoRoT and Kepler. The capability of these missions to discover terrestrial-mass planets is particularly exciting. Our method could determine if terrestrial planets with low eccentricities like the Earth are common or rare. This would provide significant constraints on theories proposed to explain the eccentricities of extrasolar planets. For example, Kepler might find many terrestrial planets with low eccentricity orbits, suggesting that the mechanisms that excite the eccentricities of giant planets are often ineffective for terrestrial mass planets. In this scenario, those terrestrial planets that do have large eccentricities might typically be accompanied by nearby giant planets, suggesting that it is the giant planets are responsible for exciting the eccentricities of terrestrial planets (Veras & Armitage 2005, 2006). Alternatively, Kepler might find that terrestrial planets are much more common than giant planets, and yet they still commonly have large eccentricities. This could arise from eccentricity excitation mechanisms that do not require giant planets, or due to interactions with previous giant planets that have since been ejected, accreted or destroyed by the star (e.g., Ford et al. 2005; Raymond et al. 2006; Mandell et al. 2007).

Our method also provides a means for studying the tidal evolution of short-period

planets. Tidal effects are likely to circularize planets with sufficiently short orbital periods. For short-period planets, we can compute the tidal circularization timescale ( $t_{\text{circ}}$ ) based on the properties of the star and planet. If there is a sharp transition between circular and eccentric orbits, then this could be used to place constraints on tidal theory (e.g., Zahn & Bouchet 1989; Melo et al. 2001; Mathieu et al. 2004). For eccentric planets with relatively short  $t_{\text{circ}}$ , it may be possible to place a lower limit on the  $Q$  factor the is related to the planet’s internal structure (e.g., Ford et al. 1999; Bodenheimer et al. 2001; Maness et al. 2007; Mardling 2007).

In a Bayesian framework, one can calculate the posterior probability distribution for the fraction of each orbit during which the planet-star separation is between an inner and outer cut-off. If the cut-offs are set to be the putative boundary of the habitable zone, then we can then ask, “What fraction of terrestrial planets are in the habitable zone for some/at least half/all of their orbit?”. The results of such investigations could have implications for the climates of potentially habitable planets, the frequency of such planets, and the design of future missions that aim to detect and characterize nearby Earth-like planets that could harbor life (e.g., Marcy et al. 2005).

We have demonstrated that it is practical to collect sufficient photons to characterize the eccentricity distribution of terrestrial extrasolar planets, but we assumed that limb-darkening parameters can be well constrained by some combination of stellar modeling and external observations. Our analytical estimates have not incorporated limb darkening effects or potential systematic uncertainties in stellar models. Future search should address both of these effects. Multi-wavelength observations (particularly in the infrared) could be particularly useful for addressing both these issues. In particular, we plan to investigate the potential for combinations of space-based detections and ground-based follow-up observations to improve the characterization of the eccentricities of transiting planets.

Finally, we note that this method for characterizing the eccentricities of terrestrial planets from transit light curves underscores the importance of developing and validating precise and accurate stellar models. Uncertainties in stellar parameters models are expected to dominate the error budget for bright target stars. The potential for systematic uncertainties due to stellar modeling will make it particularly challenging to study low eccentricity systems as a function of stellar properties. Fortunately, we these concerns would not preclude our method from being applied to terrestrial-sized planets recognizing the relatively large eccentricities typical for giant planets.

We thank G. Bakos, D. Charboneau, M. Holman, D. Latham, G. Takeda, and an anonymous referee for discussions and suggestions. Support for E.B.F. was provided by NASA



through Hubble Fellowship grant HST-HF-01195.01A awarded by the Space Telescope Science Institute, which is operated by the Association of Universities for Research in Astronomy, Inc., for NASA, under contract NAS 5-26555. Additional support for E.B.F. and D.V. was provided by the University of Florida.

## REFERENCES

- Artymowicz, P. 1992, *PASP*, 104, 769
- Bakos, G. A., et al. 2007, *ArXiv e-prints*, 705, arXiv:0705.0126
- 2008arXiv0708.0243 Barnes, J.W. 2007, *ArXiv e-prints*, 807, arXiv:0708.0243
- Basri, G., Borucki, W. J., & Koch, D. 2005, *New Astronomy Review*, 49, 478
- Beer, M. E., King, A. R., Livio, M., & Pringle, J. E. 2004, *MNRAS*, 354, 763
- Bodenheimer, P., Lin, D. N. C., & Mardling, R. A. 2001, *ApJ*, 548, 466
- Brown, T. M., Charbonneau, D., Gilliland, R. L., Noyes, R. W., & Burrows, A. 2001, *ApJ*, 552, 699
- Burke, C. J. 2008, *ArXiv e-prints*, 801, arXiv:0801.2579
- Burke, C. J., et al. 2007, *ArXiv e-prints*, 705, arXiv:0705.0003
- Butler, R. P., et al. 2006, *ApJ*, 646, 505
- Chatterjee, S., Ford, E. B., & Rasio, F. A. 2007, *ArXiv Astrophysics e-prints*, arXiv:astro-ph/0703166
- Claret, A. 2000, *A&A*, 363, 1081
- Fischer, D. A., & Valenti, J. 2005, *ApJ*, 622, 1102
- Ford, E. B., Kozinsky, B., & Rasio, F. A. 2000, *ApJ*, 535, 385
- Ford, E. B. 2006, *ApJ*, 642, 505
- Ford, E. B. 2005, *AJ*, 129, 1706
- Ford, E. B., & Gaudi, B. S. 2006, *ApJ*, 652, L137
- Ford, E. B., Lystad, V., & Rasio, F. A. 2005, *Nature*, 434, 873
- Ford, E. B., & Rasio, F. A. 2007, *ArXiv Astrophysics e-prints*, arXiv:astro-ph/0703163
- Ford, E. B., Rasio, F. A., & Sills, A. 1999, *ApJ*, 514, 411
- Gaidos, E., & Williams, D. M. 2004, *New Astronomy*, 10, 67
- Goldreich, P., & Sari, R. 2003, *ApJ*, 585, 1024

- Holman, M., Touma, J., & Tremaine, S. 1997, *Nature*, 386, 254
- Holman, M. J., et al. 2006, *ApJ*, 652, 1715
- Holman, M. J., et al. 2007, *ArXiv e-prints*, 704, arXiv:0704.2907
- Jha, S., Charbonneau, D., Garnavich, P. M., Sullivan, D. J., Sullivan, T., Brown, T. M., & Tonry, J. L. 2000, *ApJ*, 540, L45
- Juric, M., & Tremaine, S. 2007, *ArXiv Astrophysics e-prints*, arXiv:astro-ph/0703160
- Kasting, J. F., Whitmire, D. P., & Reynolds, R. T. 1993, *Icarus*, 101, 108
- Laughlin, G., & Adams, F. C. 1998, *ApJ*, 508, L171
- Laughlin, G., Marcy, G. W., Vogt, S. S., Fischer, D. A., & Butler, R. P. 2005, *ApJ*, 629, L121
- Mandel, K., & Agol, E. 2002, *ApJ*, 580, L171
- Mandell, A. M., Raymond, S. N., & Sigurdsson, S. 2007, *ApJ*, 660, 823
- Maness, H. L., Marcy, G. W., Ford, E. B., Hauschildt, P. H., Shreve, A. T., Basri, G. B., Butler, R. P., & Vogt, S. S. 2007, *PASP*, 119, 90
- Marcy, G. W., Fischer, D. A., McCarthy, C., & Ford, E. B. 2005, *Astrometry in the Age of the Next Generation of Large Telescopes*, 338, 191
- Mardling, R. A. 2007, *MNRAS*, 382, 1768
- Mathieu, R. D., Meibom, S., & Dolan, C. J. 2004, *ApJ*, 602, L121
- Melo, C. H. F., Covino, E., Alcalá, J. M., & Torres, G. 2001, *A&A*, 378, 898
- Namouni, F. 2007, *ArXiv Astrophysics e-prints*, arXiv:astro-ph/0702203
- Raymond, S. N., Mandell, A. M., & Sigurdsson, S. 2006, *Science*, 313, 1413
- Seager, S., & Mallén-Ornelas, G. 2003, *ApJ*, 585, 1038
- Sozzetti, A., Torres, G., Charbonneau, D., Latham, D. W., Holman, M. J., Winn, J. N., Laird, J. B., & O'Donovan, F. T. 2007, *ArXiv e-prints*, 704, arXiv:0704.2938
- Takeda, G., Ford, E. B., Sills, A., Rasio, F. A., Fischer, D. A., & Valenti, J. A. 2007, *ApJS*, 168, 297

- Tingley, B., & Sackett, P. D. 2005, *ApJ*, 627, 1011
- Valenti, J. A., & Fischer, D. A. 2005, *ApJS*, 159, 141
- Veras, D., & Armitage, P. J. 2006, *ApJ*, 645, 1509
- Veras, D., & Armitage, P. J. 2005, *ApJ*, 620, L111
- Williams, D. M., & Pollard, D. 2002, *International Journal of Astrobiology*, 1, 61
- Winn, J. N., Holman, M. J., & Roussanova, A. 2007, *ApJ*, 657, 1098
- Zahn, J.-P., & Bouchet, L. 1989, *A&A*, 223, 112
- Zakamska, N. L., & Tremaine, S. 2004, *AJ*, 128, 869

Table 1. Number of Planets Required to Distinguish between Distributions (Low S/N)

	$e = 0$	$e \sim R(.1)$	$e \sim R(.2)$	$e \sim R(.3)$	$e \sim R(.4)$	$e \sim R(.5)$	$e \sim R(.6)$	$e \sim U[0,1)$
$e = 0$	...	98	44	30	22	19	16	26
$e \sim R(.1)$	78	...	187	53	33	23	20	34
$e \sim R(.2)$	51	171	...	250	84	42	33	52
$e \sim R(.3)$	36	54	180	...	355	117	67	174
$e \sim R(.4)$	25	29	68	270	...	575	215	675
$e \sim R(.5)$	20	24	42	108	540	...	>1000	975
$e \sim R(.6)$	17	19	28	55	155	850	...	255
$e \sim U[0,1)$	26	29	53	117	540	850	310	...

<sup>a</sup>We list the number of planets required to distinguish an observed distribution (taken from the top row) from a theoretical distribution (taken from the left column) at the 95% confidence level based on a Kolmogorov-Smirnov test applied to  $\tau_o$ .

Table 2. Number of Planets Required to Distinguish between Distributions (High S/N)

$e = 0$	$e \sim R(.1)$	$e \sim R(.2)$	$e \sim R(.3)$	$e \sim R(.4)$	$e \sim R(.5)$	$e \sim R(.6)$	$e \sim U[0, 1)$	
$\sigma_{\tau_b} = 0.05$								
$e = 0$	...	14	11	8	7	7	6	8
$e \sim R(.1)$	17	...	47	20	12	9	9	16
$e \sim R(.2)$	11	45	...	77	33	18	17	30
$e \sim R(.3)$	8	15	72	...	158	58	34	108
$e \sim R(.4)$	7	9	21	122	...	380	127	385
$e \sim R(.5)$	6	7	14	46	335	...	725	275
$e \sim R(.6)$	5	6	11	28	99	495	...	100
$e \sim U[0, 1)$	8	11	20	67	355	305	133	...
$\sigma_{\tau_b} = 0.15$								
$e = 0$	...	29	19	13	10	9	8	11
$e \sim R(.1)$	35	...	73	23	17	11	12	22
$e \sim R(.2)$	19	65	...	88	43	23	22	38
$e \sim R(.3)$	13	23	97	...	210	70	47	125
$e \sim R(.4)$	8	14	31	145	...	465	148	480
$e \sim R(.5)$	8	11	18	60	355	...	775	375
$e \sim R(.6)$	7	8	13	37	120	545	...	135
$e \sim U[0, 1)$	10	14	26	75	410	475	175	...

<sup>a</sup>We list the number of planets required to distinguish an observed distribution (taken from the top row) from a theoretical distribution (taken from the left column) at the 95% confidence level based on a Kolmogorov-Smirnov test applied to  $\hat{\tau}_b$  with  $\sigma_{\tau_b} = 0.15$  (bottom) and 0.05 (top).

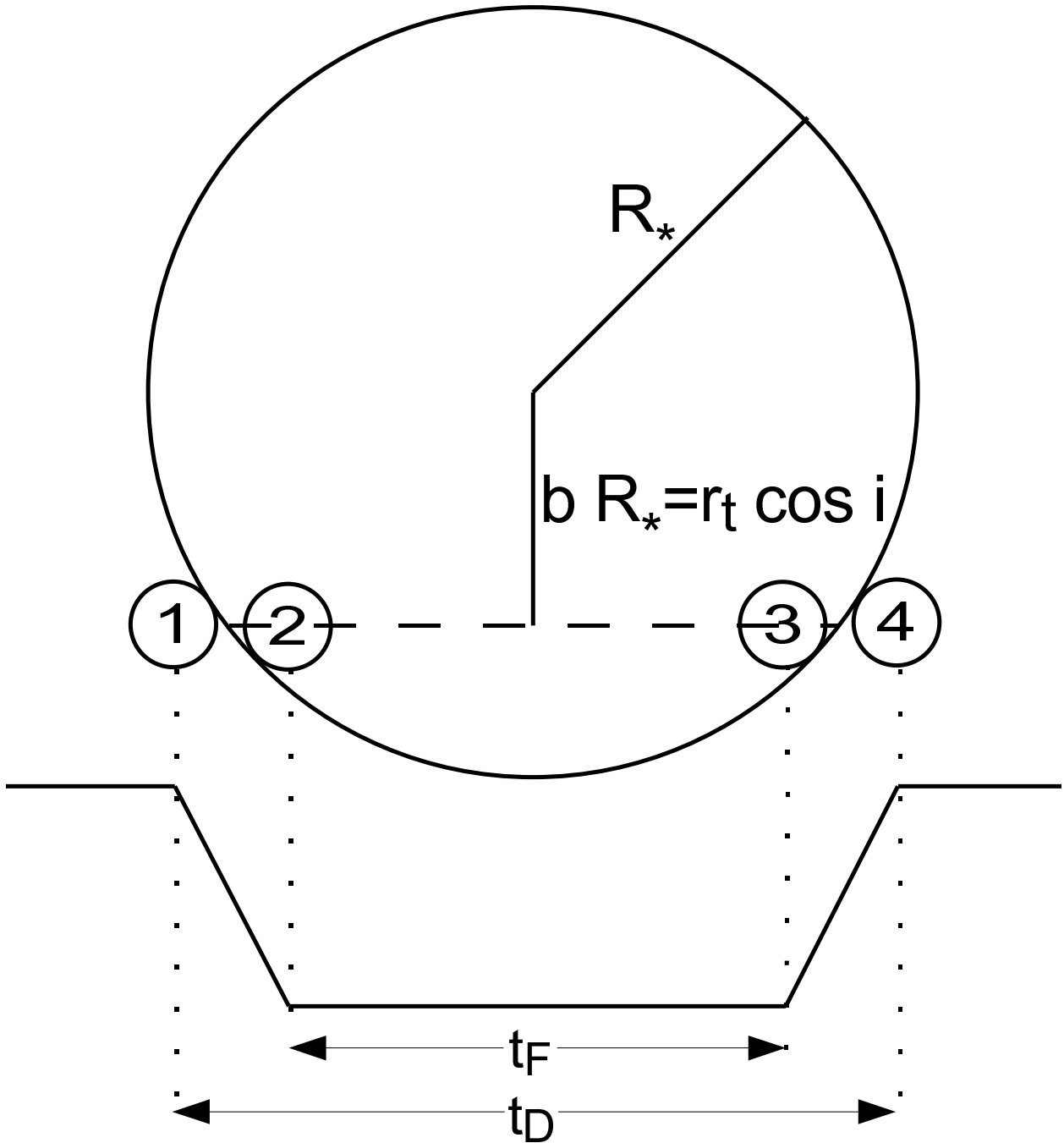


Fig. 1.— Geometry of Transit: Here we illustrate the path (dashed line) of a planet (small circles) as it transits a star (large circle). The vertical dotted lines connect the planet to the schematic light curve (solid curve) at the time of each of the four points of contact. Measuring the times of all four points of contact allows for a measurement of the impact parameter ( $b$ ) and significantly increases the precision of the constraint on the planet’s eccentricity. If only the total transit duration ( $t_D$ ) is measured, then the eccentricity distribution can still be constrained for a larger population of transiting planets.

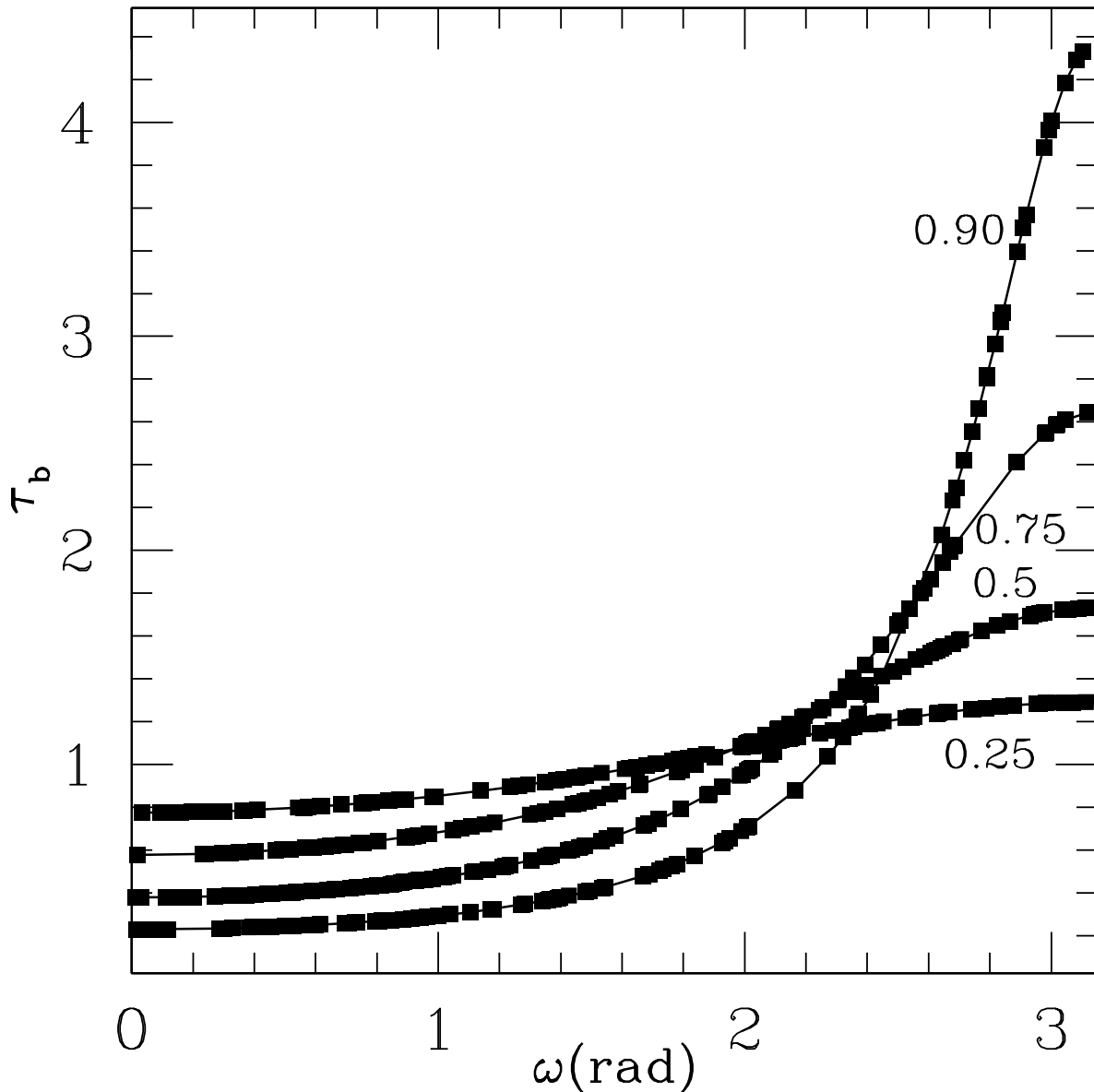


Fig. 2.— Transit Duration as a function of eccentricity ( $e$ ) and argument of periastron ( $\omega$ ): The vertical axis shows  $\tau_b$ , the ratio of the actual transit duration to the transit duration for a similar planet on a circular orbit (with the same sizes, orbital period and impact parameter). The curves show the analytic approximation for the transit duration (Eqn. 1) for four values of eccentricity, 0.25, 0.5, 0.75, 0.9. The points are the exact durations for a planet on a Keplerian orbit. For a planet on a circular orbit,  $\tau_b = 1$ , but for eccentric planets  $\tau_b$  can be larger (for planets that transit near apocenter) or smaller (for planets that transit near pericenter). Thus, a measurement of the transit duration can be used to constrain a combination of  $e$  and  $\omega$  (measured from the direction of the observer), as well as to place a lower limit on the eccentricity.



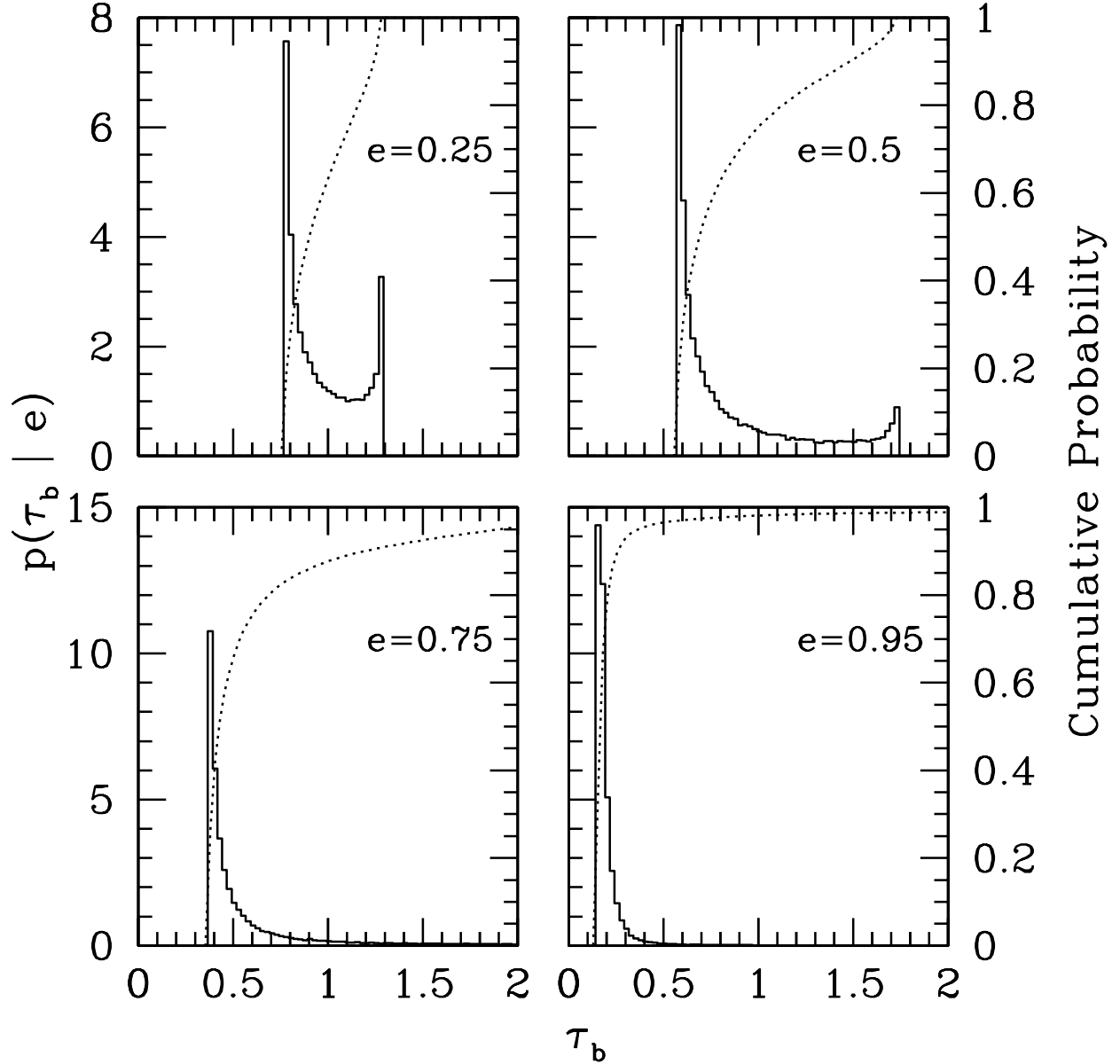


Fig. 3.— Probability Distribution for Transit Duration at a given eccentricity ( $e$ ): Here we show the probability distribution (solid histogram) for  $\tau_b$  for an ensemble of planets with a single fixed eccentricity, assuming a uniform distribution of the argument of pericenter and an isotropic distribution of inclinations. The dotted curves are the cumulative probability distributions. For large eccentricities, there is a small fraction of very long transits ( $\tau_b > 2$  off the scale).

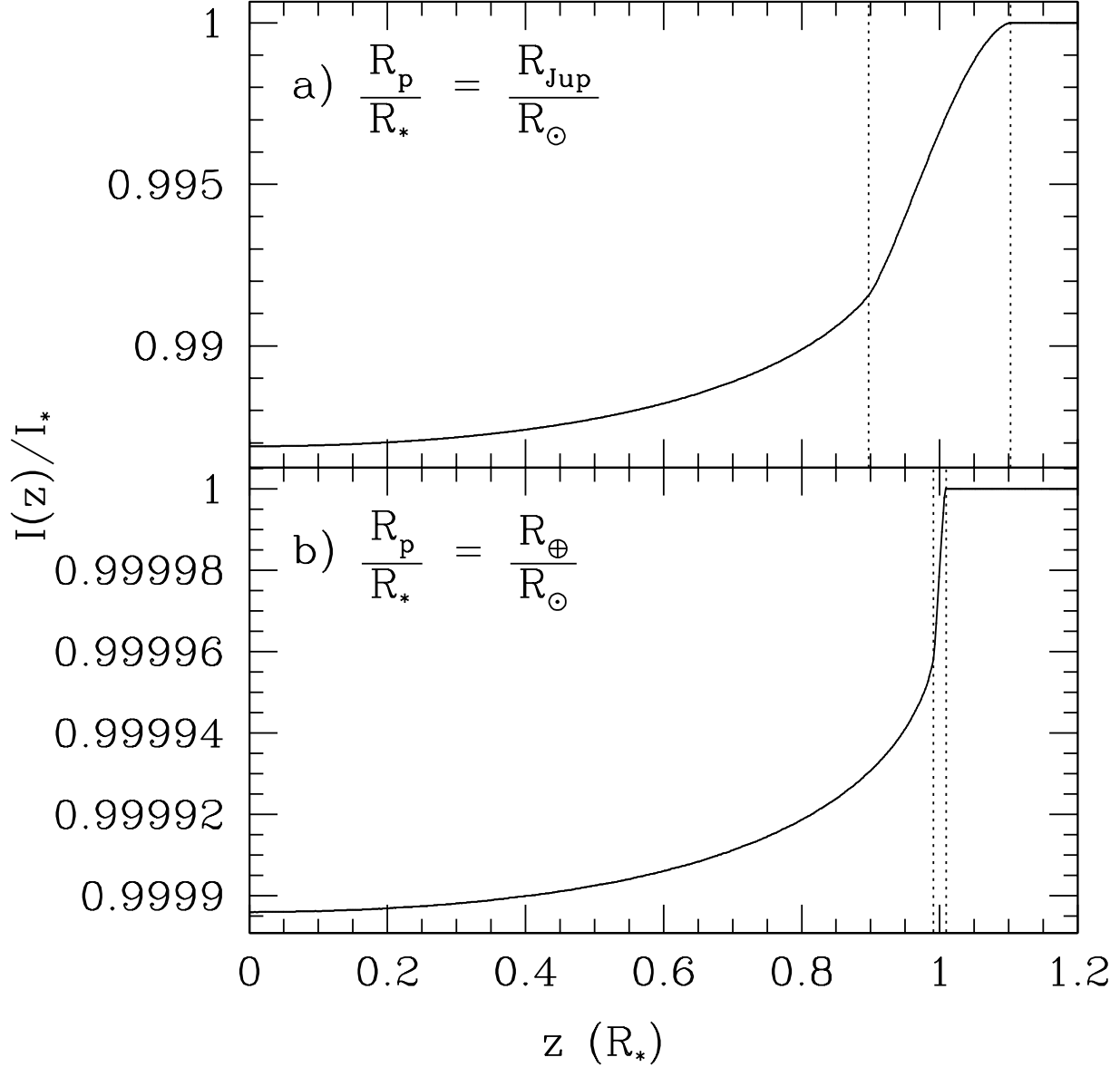


Fig. 4.— Transit light curves illustrating effects of limb-darkening. Here we show the observed intensity ( $I(z)$ ; normalized to total stellar flux,  $I_*$ ) as a function of  $z$ , the projected separation from the center of the star (measured in stellar radii). The vertical dotted lines indicate the points of contact. For this illustration, we adopt a quadratic limb-darkening model (Mandel & Agol 2002) and limb darkening coefficients of  $\gamma_1 = 0.4382$  and  $\gamma_2 = 0.2924$  based on ATLAS models for solar-like star in V band (Claret 2000). *Top*: For a Jupiter-sized planet, *Bottom*: For an Earth-sized planet.

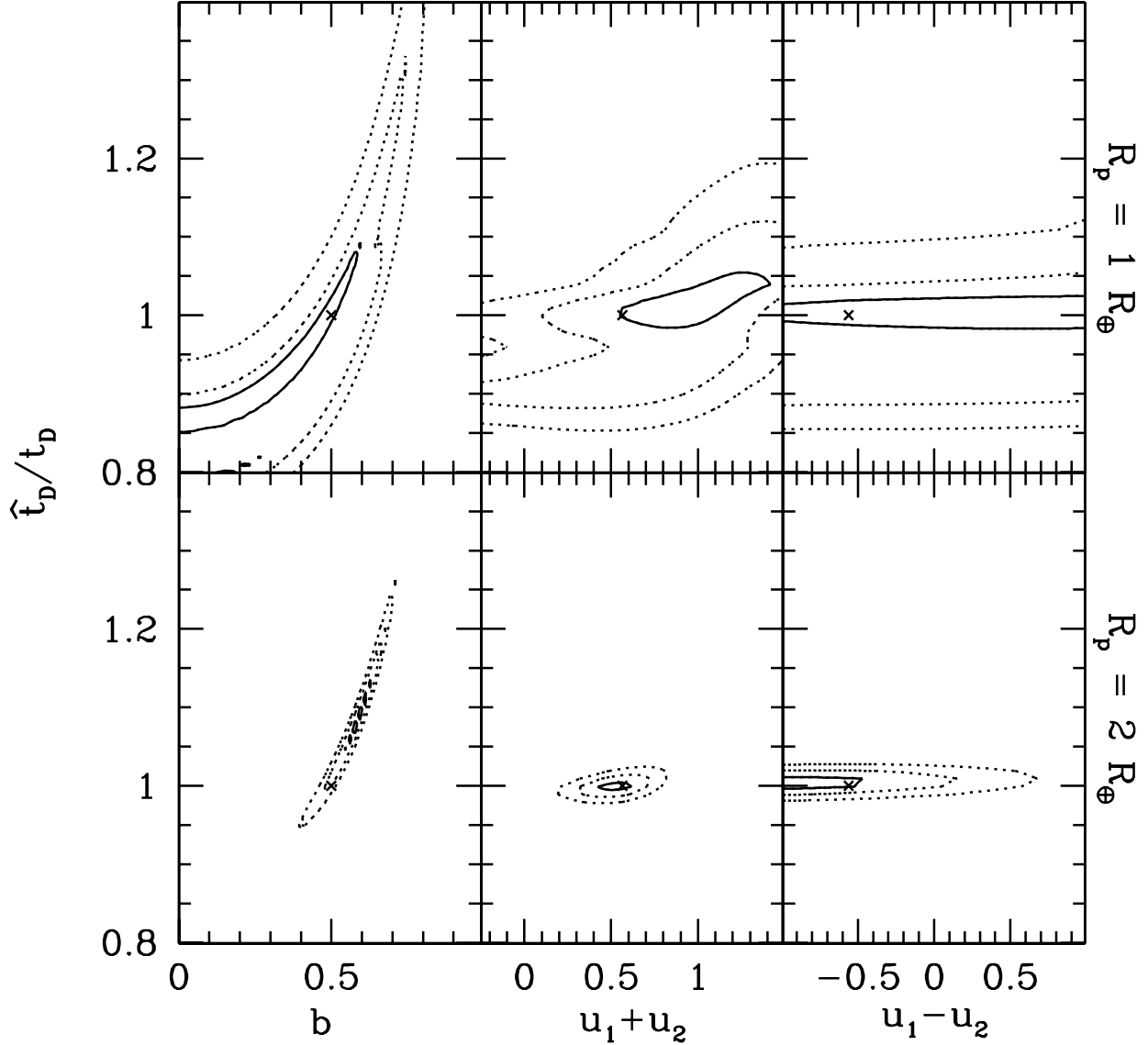


Fig. 5.— Correlations between transit duration and impact parameter or limb darkening coefficients. Here we shows contour of constant  $\Delta\chi^2 = 1, 4,$  and  $9$  with  $\hat{t}_D/t_D$  (the ratio of the model transit duration to the actual transit duration) on the  $y$ -axis. The various collumns have  $x$ -axes of the impact parameter ( $b$ ; left), the sum of the quadratic limb darkening coefficients ( $u_1 + u_2$ ; center), and the difference of the quadratic limb darkening coefficients ( $u_1 - u_2$ ; right). The top row shows a  $1 R_\oplus$  planet and the bottom row shows a  $2R_\oplus$  planet, both assumed to be at 1 AU from a solar mass star.

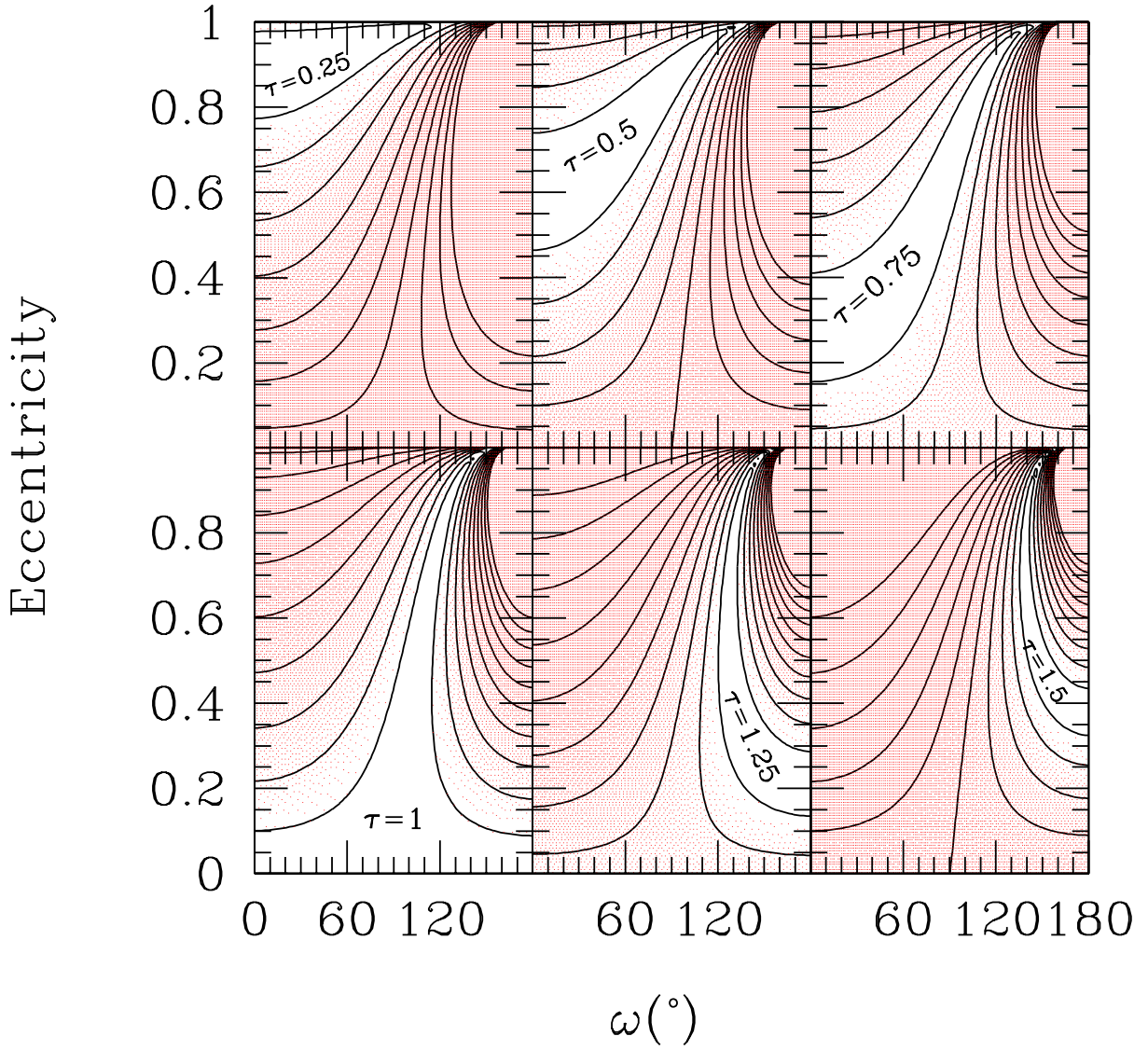


Fig. 6.— Posterior Joint Probability Distribution for  $e$  and  $\omega$ : Here we consider the eccentricity constraint based on the measured value of  $\tau_b$  for an individual planet with a measured impact parameter. We show contours equivalent to 1, 2, 3,...- $\sigma$  bounds on the combination of eccentricity and argument of pericenter. The shaded regions are excluded by the measurement of  $\tau_b$ . The panels correspond to  $\tau_b = 0.25$  (top left), 0.5 (top center), 0.75 (top right), 1 (bottom left), 1.25 (bottom center), and 1.5 (bottom right). Here we assume that the detection probability (given that a transit occurs) is independent of transit duration and that the measurement of  $\hat{\tau}_b$  is normally distributed and has a standard deviation,  $\sigma_{\tau_b} = 0.1$ .

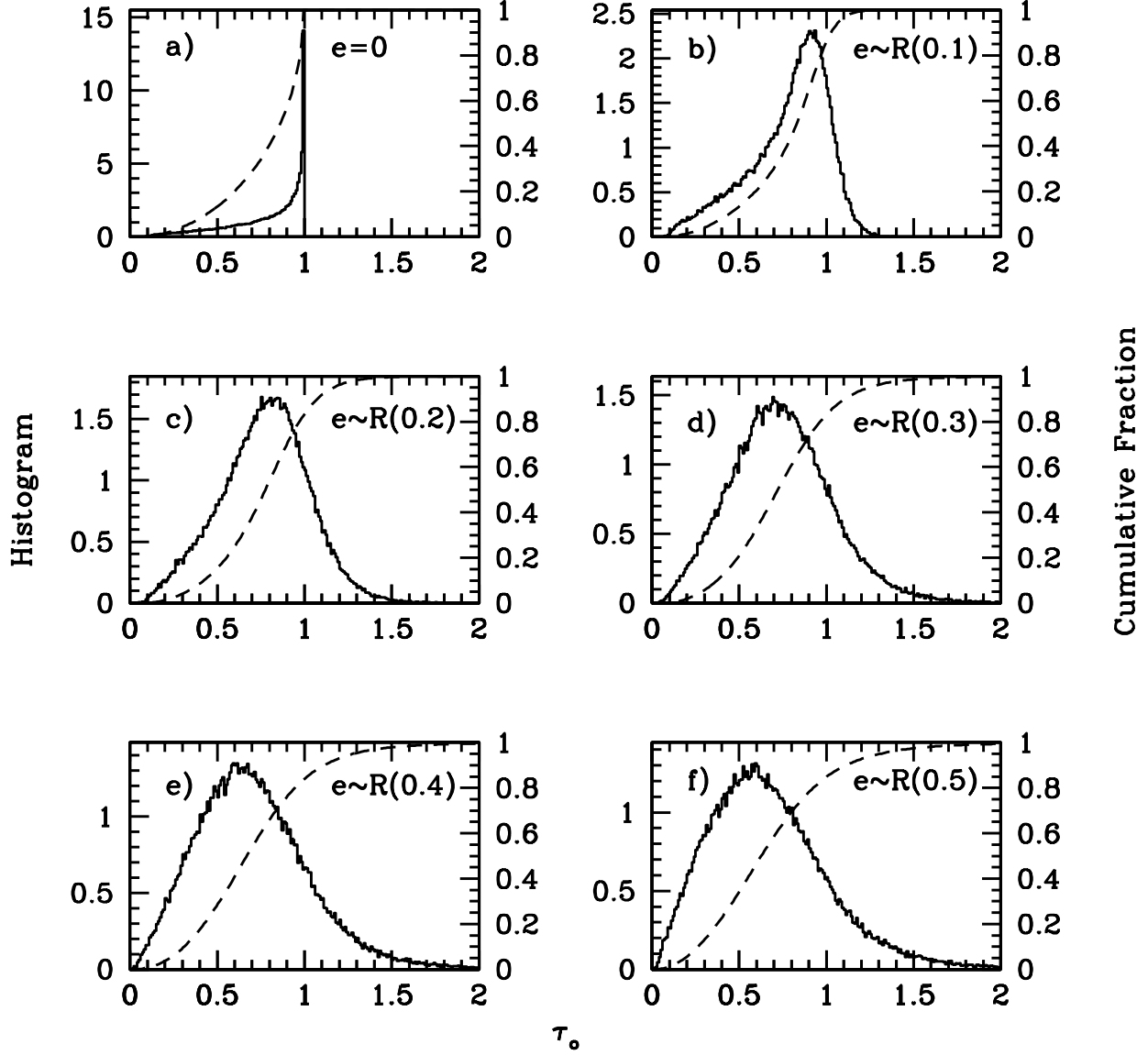


Fig. 7.— Distribution of Transit Duration for Various Eccentricity Distributions: We show histograms (solid curves) and cumulative distributions (dashed curves) of  $\tau_o$ , the ratio of the observed transit duration to that expected for the same planet, star, and orbital period, but a circular orbit and a central transit. Panel a corresponds to only circular orbits, panels b-f correspond to a Rayleigh eccentricity distribution with Rayleigh parameter of 0.1 (b), 0.2 (c), and 0.3 (d), 0.4 (e), and 0.5 (f).

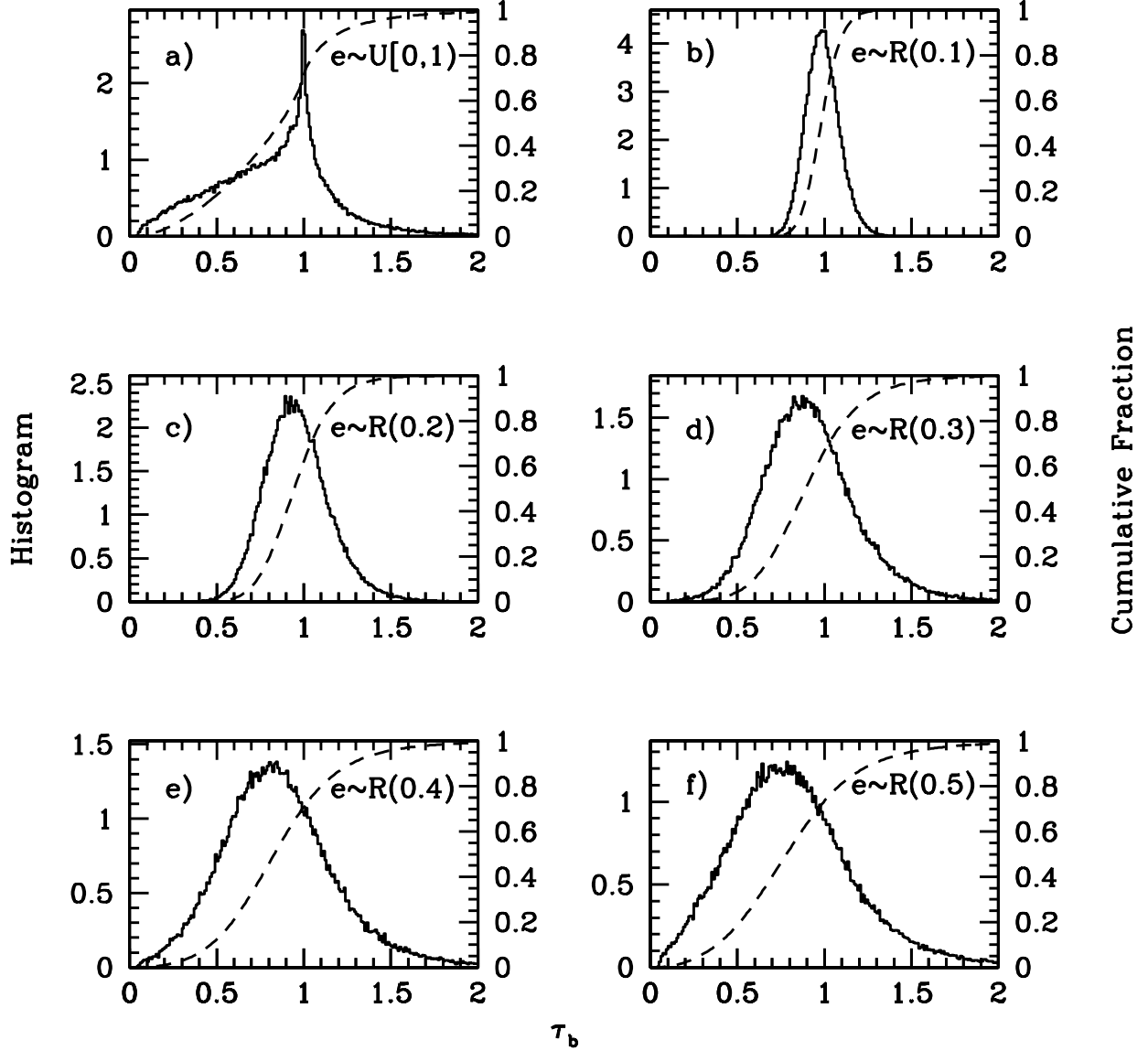


Fig. 8.— Distribution of Transit Duration for Various Eccentricity Distributions: We show histograms (solid curves) and cumulative distributions (dashed curves) of  $\tau_b$ , the ratio of the observed transit duration to that expected for a similar planet, star, impact parameter, and orbital period, but a circular orbit. Panel a corresponds to a uniform eccentricity distribution, panels b-f correspond to a Rayleigh eccentricity distribution with Rayleigh parameter of 0.1 (b), 0.2 (c), and 0.3 (d), 0.4 (e), and 0.5 (f).

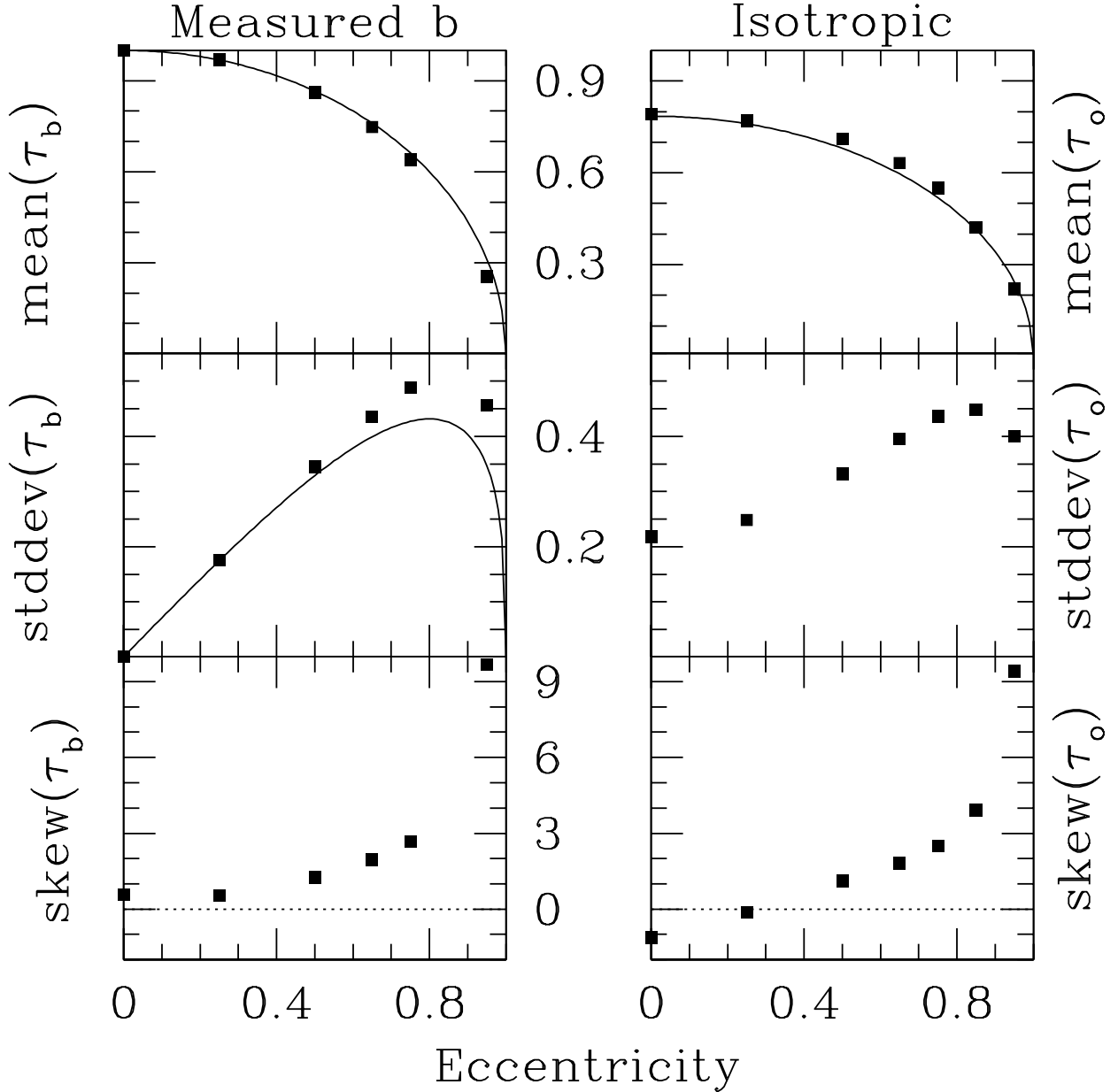


Fig. 9.— Moments of the Normalized Transit Duration Distribution: Here we consider several ensembles of transiting planets, each with a single fixed eccentricity. For each eccentricity, we calculate the distribution of  $\tau_b$  (left; for transits with measured impact parameters) and  $\tau_o$  (right; for transits without measured impact parameters). Here we plot the mean, standard deviation, and skewness for both both  $\tau_b$  and  $\tau_o$  for each eccentricity. We show analytic approximations with curves when available.

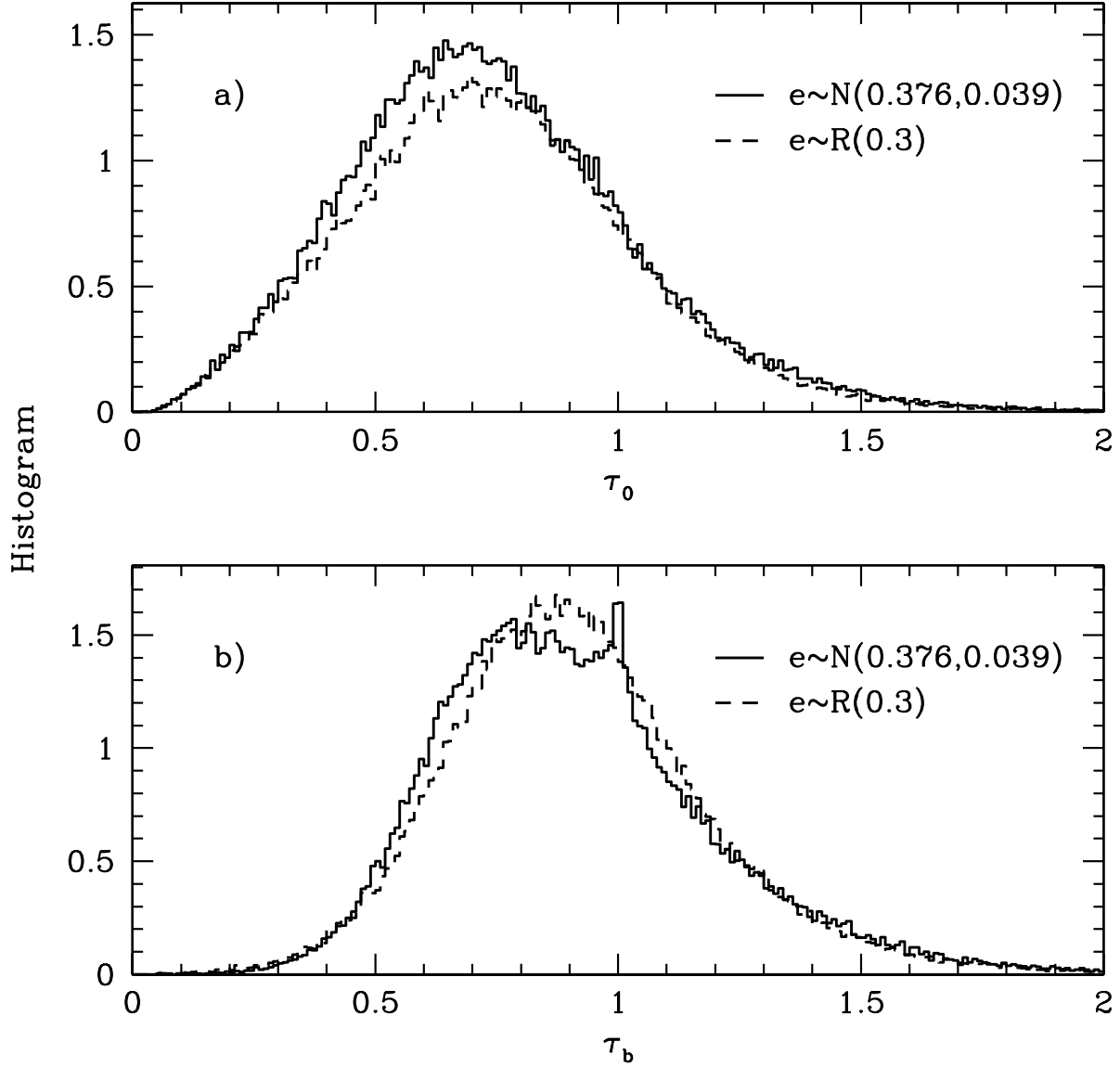


Fig. 10.— Distribution of Transit Duration for Eccentricity Distributions with Common Mean and Variance: *Top*: Histograms of  $\tau_o$ , the ratio of the observed transit duration to that expected for the same planet, star, and orbital period, but a circular orbit and a central transit. We show results for two eccentricity distributions: normal (solid) and Rayleigh (dashed). The mean and variance of the normal distribution have been chosen to match that of a Rayleigh distribution with Rayleigh parameter 0.3. The resulting distributions of  $\tau_o$  are so similar that it would be extremely difficult to distinguish between these eccentricity distributions. *Bottom*: Same as above, but for histograms of  $\tau_b$ , the ratio of the observed transit duration to that expected for a similar planet, star, impact parameter, and orbital period, but a circular orbit. Again, the distributions of  $\tau_b$  are too similar to distinguish between the eccentricity distributions.